Original paper

Garnet pyroxenite in the Biskupice peridotite, Bohemian Massif: anatomy of a Variscan high-pressure cumulate

L. Gordon MEDARIS, Jr.[1*], Emil JELÍNEK[2], Brian L. BEARD[1], John W. VALLEY[1], Michael J. SPICUZZA[1], Ladislav STRNAD[3]

[1] *Department of Geoscience, University of Wisconsin-Madison, 1215 West Dayton, Madison, WI 53706, USA; medaris@geology.wisc.edu*
[2] *Institute of Geochemistry, Mineralogy and Mineral Resources, Charles University, Albertov 6, 128 43 Prague 2, Czech Republic*
[3] *Laboratories of Geological Institutes, Charles University, Albertov 6, 128 43 Prague 2, Czech Republic*
[*] *Corresponding author*

A strongly layered garnet pyroxenite, consisting of cm-scale layers of garnetite, garnet orthopyroxenite, garnet clinopyroxenite, and websterite, occurs in the Biskupice garnet peridotite, which is located in migmatitic gneiss of the Gföhl Assemblage in the Vysočina District, western Moravia. Major- and trace-element compositions and REE patterns of minerals and layers in the pyroxenite are consistent with origin of the layers by HT–HP crystallization and accumulation of variable proportions of garnet, orthopyroxene, and clinopyroxene. The present compositions of the minerals (pyrope-rich garnet, low-Al, low-Ca enstatite and low-Al, high-Ca diopside) are the result of extensive subsolidus re-equilibration at ~900 ºC and ~37 kbar, during the Variscan (332 Ma) Orogeny. Neodymium and strontium isotopic values (ε^{335}_{Nd}, +1.8 to +2.1; $(^{87}Sr/^{86}Sr)_{335}$, 0.7049) and negative HFSE anomalies indicate a crustal component in the melt from which the layers crystallized. Most garnet pyroxenites and eclogites in Gföhl garnet peridotites are thought to have formed by HT–HP crystallization from silicate melts containing crustal components, and the Biskupice garnet pyroxenite is an excellent example of such a petrogenetic process.

Keywords: pyroxenite, Moldanubian, geochemistry, Sr and Nd isotopes, O isotopes, P–T conditions
Received: 17 October, 2012; accepted: 6 March, 2013; handling editor: S. Vrána

1. Introduction

Garnet pyroxenite and eclogite constitute a small fraction of lithospheric mantle, appearing at the surface of the Earth as layers and lenses in peridotite massifs and as xenoliths in kimberlite and alkali basalt. Although garnet pyroxenite and eclogite are volumetrically minor, they are petrologically important in providing evidence for the geochemical evolution of the mantle. Numerous hypotheses have been proposed for the origin of mantle pyroxenite and eclogite, among which the two end-member scenarios are derivation from subducted oceanic crust that was tectonically incorporated into the mantle or high-pressure crystallization from melts migrating through the mantle (for reviews, see Jacob 2004; Griffin and O'Reilly 2007; Gonzaga et al. 2010).

Garnet pyroxenite and eclogite layers, lenses, and veins occur in garnet peridotite bodies in the Gföhl Assemblage, which is the uppermost structural unit in the Moldanubian Zone of the Variscan Massif. Geochemical data and modelling indicate that such pyroxenite and eclogite originated by high-pressure crystallization of garnet and clinopyroxene (± trapped liquid) from melts derived from subducted oceanic crust (Beard et al. 1992; Becker 1996; Medaris et al. 1995, 2006), although some kyanite eclogite is thought to represent subducted oceanic crust (Becker 1996; Obata et al. 2006).

In the course of our investigation of ultramafic rocks in the Gföhl Assemblage, we discovered a strongly layered garnet pyroxenite in the Biskupice garnet peridotite (Fig. 1). Although some degree of layering is present in some Gföhl pyroxenite and eclogite samples, such strong development is exceptional and deserves close inspection. Accordingly, a detailed investigation has been carried out on the mineralogy, petrology, and geochemistry of the Biskupice layered garnet pyroxenite, and in this short communication we report results which bear on the origin of this pyroxenite in particular, and on geochemical processes operating in the mantle in general.

2. Geological setting

A segment of the Gföhl Assemblage, consisting of granulite, migmatitic gneiss, and leucocratic migmatite (Hasalová et al. 2008), is located in the Vysočina District, western Moravia, between the 335–342 Ma Třebíč durbachite Pluton on the northwest (Holub et al. 1997; Kotková et al. 2010; Kusiak et al. 2010), Bíteš orthogneiss of the Moravian Zone on the northeast, and Permian sedimen-

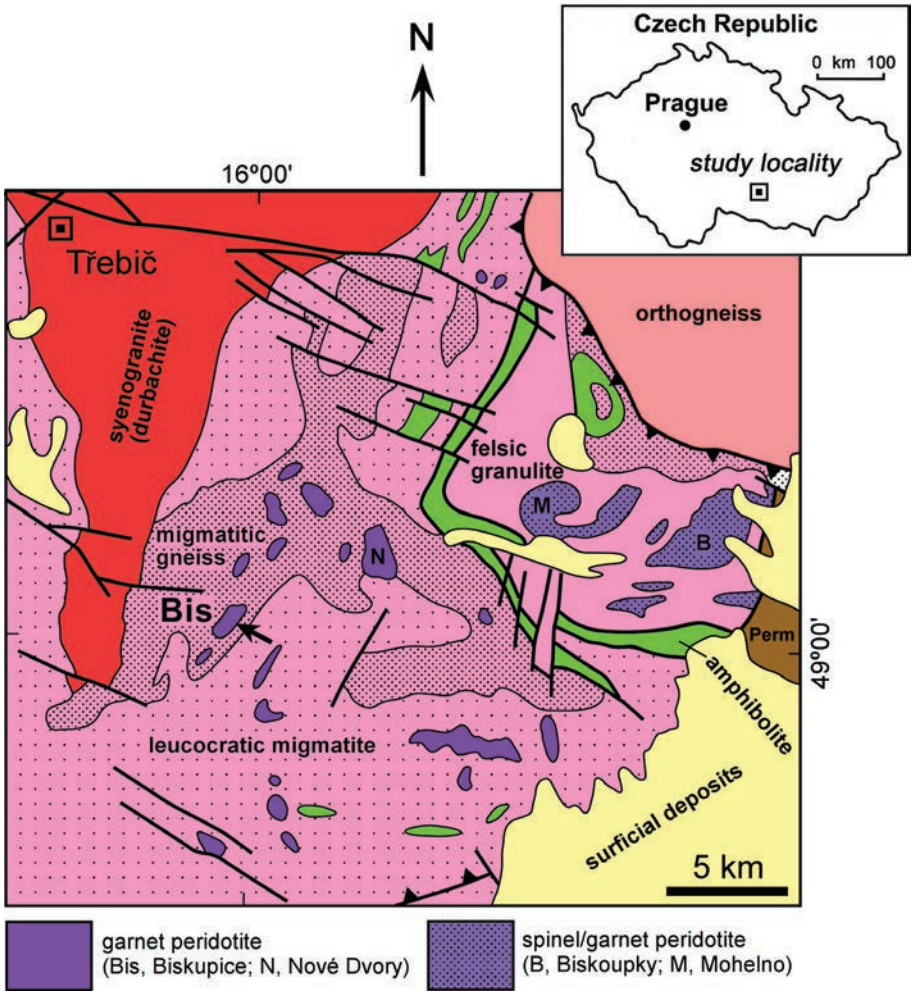

Fig. 1 Simplified geological map of the Třebíč area, Vysočina District, western Moravia, modified from the 1:500,000 Geological Map of the Czech Republic (Cháb, et al. 2007). The Mohelno (M) and Nové Dvory (N) types of peridotite are designated by different colors and patterns, as indicated in the legend beneath the figure. Locality of the Biskupice peridotite is labeled (Bis) and indicated by an arrow. Study area is shown in the inset.

tary rocks and surficial deposits on the southeast (Fig. 1). Two types of peridotite occur in this Gföhl Terrane, exemplified by the Mohelno and Nové Dvory peridotites (Fig. 1; Medaris et al. 1990, 2005). The *Mohelno type* is located in high-pressure felsic granulite, with which it has concordant contacts, and consists predominantly of spinel peridotite, with garnet peridotite occurring only within a few meters of contacts with the surrounding granulite (Kusbach et al. 2012). Centimeter-scale spinel pyroxenite layers and lenses occur in spinel peridotite, but neither garnet pyroxenite nor eclogite have been found so far in the Mohelno type of peridotite. The *Nové Dvory type* is in fault contact with surrounding migmatitic gneiss or leucocratic migmatite, consists entirely of garnet peridotite, and contains layers and lenses of garnet pyroxenite and eclogite on a centimeter- to decameter-scale (Medaris et al. 1995, 2006; Nakamura et al. 2004).

The Mohelno type of peridotite contains high-Al orthopyroxene and yields a low pressure/temperature (P/T) field gradient; in contrast, the Nové Dvory type contains low-Al orthopyroxene and yields a high P/T field gradient. The two types of peridotite are also geochemically distinct, with the Mohelno type being more depleted in incompatible elements compared to the Nové Dvory type (Medaris et al. 2005).

The layered garnet pyroxenite of this investigation occurs in the Biskupice garnet peridotite, which has characteristics of the Nové Dvory type and is located ~7 km southwest of the Nové Dvory peridotite, itself (Fig. 1). The Biskupice peridotite is very poorly exposed, although small samples of garnet pyroxenite, eclogite, and quartz–kyanite eclogite, which are more resistant to weathering than peridotite, were collected from soils overlying the peridotite, as was the layered garnet pyroxenite studied here.

3. Sample description

The sample of Biskupice layered garnet pyroxenite is ~10×10 cm in size, with centimeter-scale layers of garnet clinopyroxenite (layers A, C, E, and G), garnet orthopyroxenite (layers B and D), garnetite (layer F), and garnet websterite (layer H) (Fig. 2). The contacts of the layers are relatively sharp, and the proportions of the three principal phases in each layer, garnet, clinopyroxene, and orthopy-

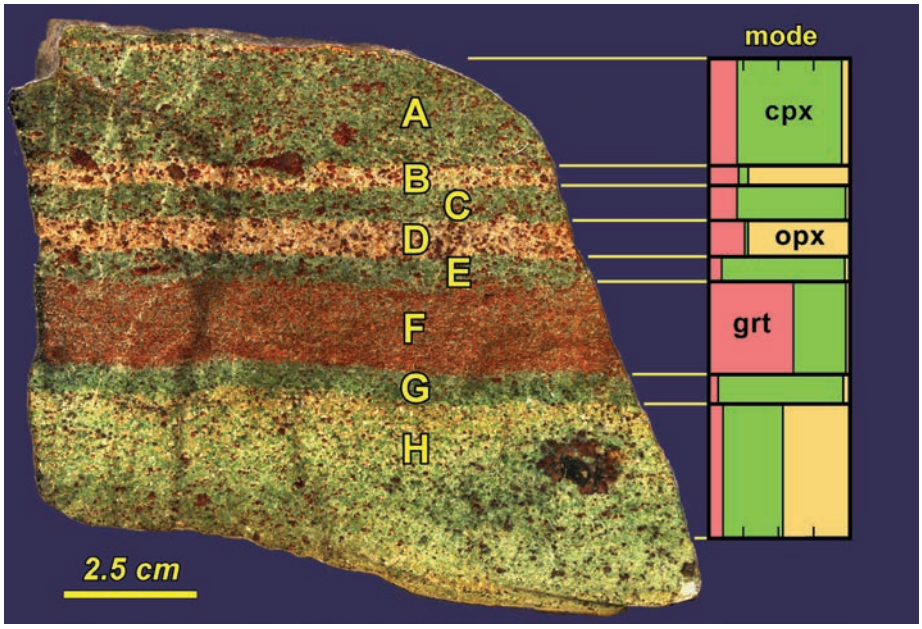

Fig. 2 The Biskupice garnet pyroxenite: layers A, C, E, and G are garnet clinopyroxenite; layers B and D, garnet orthopyroxenite; layer F, garnetite; layer H, garnet websterite. Modes of each layer are illustrated in the right-hand column: red, garnet; green, clinopyroxene; yellow, orthopyroxene; the mode shown for layer H is the mean for three domains within the layer.

roxene, are relatively constant in most layers, except for small, local domains of concentrated garnet in layers A, B, and E and a larger garnet- and ilmenite-rich domain in layer H (Fig. 2). The modes of each layer are given in Tab. 1. In contrast to the other layers, layer H displays some modal variation (garnet, 9–12 vol. %; clinopyroxene, 34–52 vol. %; orthopyroxene, 35–52 vol. %).

All layers exhibit a fine-grained, granoblastic texture, with straight to slightly curved grain boundaries and, locally, the development of 120º grain boundaries (Fig. 3). The grain-shape fabric is largely isotropic, although there is a slight tendency for garnet grains to be elongated parallel to layering.

Garnet, clinopyroxene, and orthopyroxene are accompanied by small, intergranular accessory grains of ilmenite (0.1–0.7 vol. %; absent in layer G) and rutile (0.1–0.4 vol. %; absent in layers C and D) (Fig. 4). Amphibole occurs in every layer (0.6–4.1 vol. %) as thin rims on garnet (Fig. 3) and associated with ilmenite and rutile (Fig. 4).

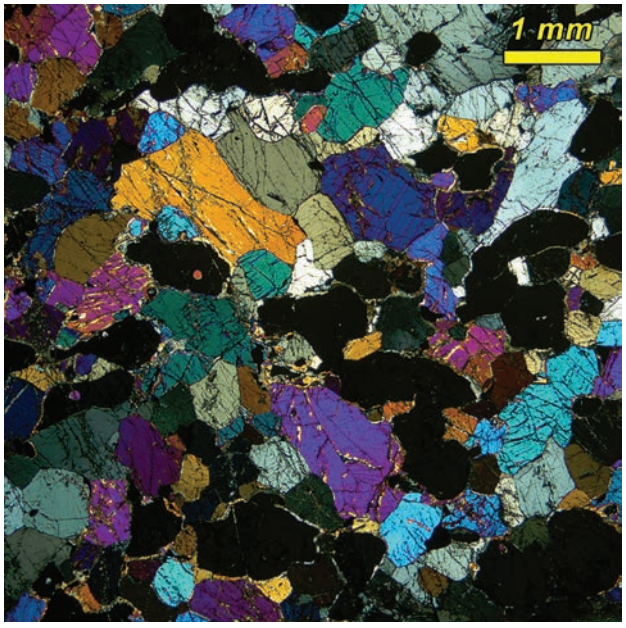

Fig. 3 Photomicrograph (crossed polarizers) of layer H, illustrating granoblastic texture. Clinopyroxene and orthopyroxene are birefringent, garnet is black (isotropic), and bright fringes on garnet are amphibole.

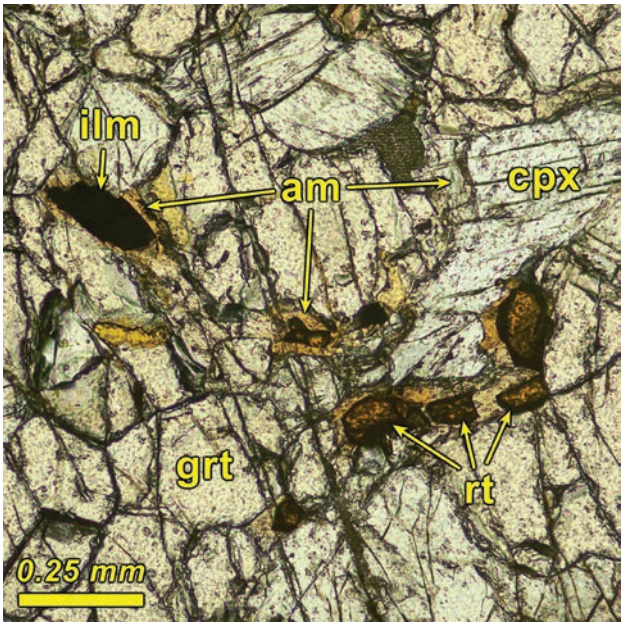

Fig. 4 Photomicrograph (plane polarized light) of layer H, illustrating the occurrence of ilmenite (ilm), rutile (rt), and intergranular amphibole (am). Garnet (grt) and clinopyroxene (cpx) are also in the field of view.

Tab. 1 Layer modes and calculated major-element compositions

Layer	A	B	C	D	E	F	G	H1	H2	H3
vol. %										
grt	20.3	20.7	20.3	26.2	9.0	59.5	6.8	11.6	9.4	9.9
opx	4.6	71.4	2.4	71.7	2.5	0.9	2.4	52.1	41.3	34.9
cpx	73.6	6.9	72.7	0.8	83.7	36.4	87.9	33.9	46.3	52.1
amph	0.9	0.9	3.9	0.6	4.1	2.6	2.5	2.0	2.8	2.9
rt	0.1	0.1	0.0	0.0	0.1	0.4	0.3	0.3	0.1	0.1
ilm	0.5	0.1	0.7	0.7	0.6	0.2	0.0	0.1	0.1	0.1
Sum	100.0	100.0	100.0	100.0	100.0	100.0	100.0	100.0	100.0	100.0
wt. %										
SiO_2	50.68	52.36	50.56	51.22	52.19	45.33	52.89	53.16	53.43	53.21
TiO_2	0.60	0.29	0.64	0.60	0.62	0.73	0.47	0.49	0.19	0.22
Al_2O_3	6.31	5.76	6.51	6.94	4.33	15.02	3.48	4.03	3.74	3.93
Cr_2O_3	0.34	0.18	0.35	0.10	0.15	0.02	0.36	0.34	0.36	0.39
FeO*	7.18	10.50	7.16	11.91	6.08	11.61	5.55	8.51	7.57	7.24
MnO	0.13	0.17	0.12	0.20	0.11	0.28	0.10	0.13	0.12	0.11
MgO	16.88	27.70	16.61	27.22	16.43	15.80	16.43	24.52	22.90	21.87
CaO	17.27	2.95	17.22	1.78	18.95	10.78	19.47	8.37	11.07	12.33
Na_2O	0.60	0.09	0.83	0.02	1.14	0.43	1.24	0.45	0.62	0.69
K_2O	0.00	0.00	0.01	0.00	0.00	0.00	0.00	0.00	0.00	0.00
Sum	100.00	100.00	100.00	100.00	100.00	100.00	100.00	100.00	100.00	100.00
Mg#	80.7	82.5	80.5	80.3	82.8	70.8	84.1	83.7	84.4	84.3

* Total Fe as FeO
Mg# = 100 × Mg/(Mg + Fe)

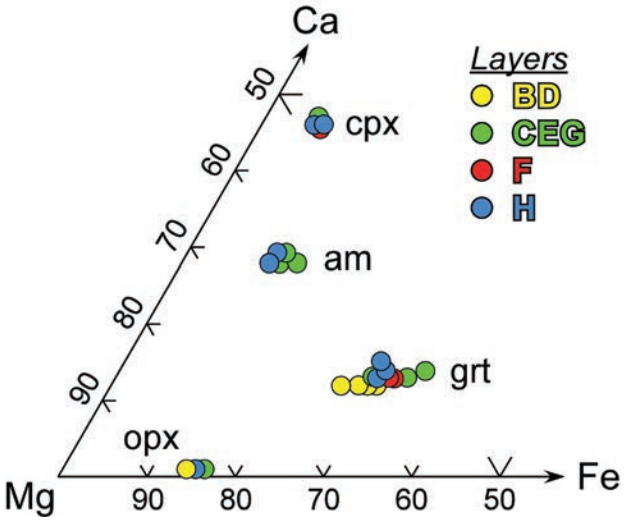

Fig. 5 Compositions of garnet (grt), clinopyroxene (cpx), orthopyroxene (opx), and amphibole (am) in the triangle Ca–Mg–Fe on an atomic basis. Data symbols are color coded according to layer occurrence: yellow, orthopyroxenite; green, clinopyroxenite; blue, websterite; red, garnetite. Minerals in layer A were not analyzed.

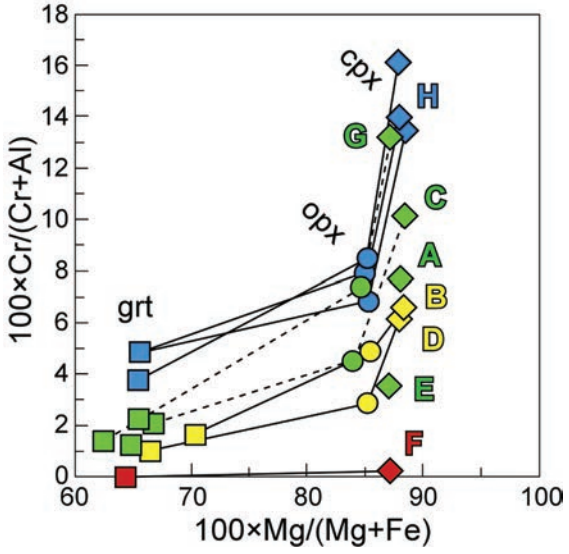

Fig. 6 Cr# [100×Cr/(Cr + Al)] *vs.* Mg# [100×Mg/(Mg + Fe)] for garnet (squares), orthopyroxene (circles), and clinopyroxene (diamonds). Symbols are color coded as in Fig. 5.

Tab. 2 Electron-microprobe analyses of garnet (means, grain cores)

Layer	A	B	C	D	E	F	G	H
wt. %								
SiO_2	41.10	41.12	41.01	40.94	40.70	40.70	40.79	40.62
TiO_2	0.22	0.15	0.18	0.21	0.18	0.17	0.20	0.19
Al_2O_3	21.57	22.34	21.86	21.98	21.86	22.34	21.86	20.98
Cr_2O_3	0.75	0.58	0.69	0.33	0.42	0.01	0.48	1.60
FeO*	14.87	12.96	14.32	14.64	15.23	15.24	16.34	14.59
MnO	0.36	0.41	0.39	0.38	0.37	0.38	0.47	0.42
MgO	15.83	17.28	16.19	16.32	15.77	15.36	15.26	15.60
CaO	4.92	4.73	5.05	4.61	5.12	5.09	4.98	5.69
Sum	99.62	99.56	99.68	99.42	99.64	99.29	100.38	99.69
cations per 12 oxygen atoms								
Si	3.023	2.997	3.008	3.009	2.999	3.004	2.998	3.002
Ti	0.012	0.008	0.010	0.012	0.010	0.009	0.011	0.010
Al	1.869	1.919	1.890	1.903	1.898	1.944	1.894	1.827
Cr	0.043	0.033	0.040	0.019	0.024	0.001	0.028	0.094
Fe	0.914	0.790	0.879	0.900	0.938	0.940	1.005	0.902
Mn	0.023	0.026	0.024	0.024	0.023	0.023	0.029	0.026
Mg	1.735	1.877	1.770	1.788	1.732	1.690	1.672	1.718
Ca	0.388	0.369	0.397	0.363	0.404	0.403	0.392	0.450
Sum	8.008	8.019	8.017	8.018	8.029	8.015	8.030	8.028
% Alm**	29.9	25.8	28.6	29.3	30.3	30.8	32.4	29.1
% Sps**	0.7	0.8	0.8	0.8	0.7	0.8	0.9	0.8
% Prp**	56.7	61.3	57.7	58.2	55.9	55.3	54.0	55.5
% Grs**	12.7	12.1	12.9	11.8	13.0	13.2	12.7	14.5
Mg#	65.5	70.4	66.8	66.5	64.9	64.3	62.5	65.6

* total Fe as FeO

** Alm, almandine; Sps, spessartine; Prp, pyrope; Grs, grossularite

Mg# = 100 × Mg/(Mg + Fe)

4. Mineral compositions

The major- and minor-element compositions of minerals in each layer were determined by electron microprobe (details of analytical techniques are given in the Appendix). Minerals in each layer are relatively uniform in composition, except for a slight change at the rims of grains, *i.e.* a decrease in Mg# (Mg# = 100×Mg/[Mg + Fe]) of garnet (~5 mol. %), an increase in Al_2O_3 of orthopyroxene (~0.1–0.2 wt. %), and a decrease in Na_2O in clinopyroxene (~0.1–0.3 wt. %). Such compositional variations are commonly developed in garnet, orthopyroxene, and clinopyroxene of peridotite massifs during cooling and decompression (Medaris and Carswell 1990). The mean compositions of grain cores are given in Tabs 2–5.

Garnet is pyrope rich, with a compositional range over all the layers of Prp 54–61, Alm 26–32, Sps 0.7–0.9, and Grs 12-14 (Tab. 2). The TiO_2 contents are low, varying from 0.15 to 0.22 wt. %. The Mg# in garnet overlaps in most layers between 64 and 67, with garnet in clinopyroxenite G yielding the lowest value at 62.5 and garnet in orthopyroxenite B, the highest value at 70.4 (Figs 5–6). Garnet contains 0.33 to 0.75 wt. % Cr_2O_3 in clinopyroxenite and orthopyroxenite, and 1.60 wt. % Cr_2O_3 in websterite, but surprisingly, only 0.01 wt. % Cr_2O_3 in garnetite layer F (Tab. 2). The Cr variation among layers is illustrated in Fig. 6, where Cr contents are expressed in terms of Cr# (Cr# = 100×Cr/[Cr + Al]).

Orthopyroxene is low-Ca and low-Al enstatite, containing 0.28–0.39 wt. % CaO and 0.65–0.98 wt. % Al_2O_3 (Tab. 3, Fig. 5). Mg# varies slightly from 83.9 to 85.5, with the highest value occurring in orthopyroxenite B, as is the case for garnet.

Clinopyroxene is low-Na diopside, containing 0.82–1.29 wt. % Na_2O (Tab. 4). The Al_2O_3 contents vary from

Tab. 3 Electron-microprobe analyses of orthopyroxene (means, grain cores)

Layer	B	C	D	G	H
wt. %					
SiO_2	56.15	55.65	56.22	55.74	55.86
TiO_2	0.06	0.07	0.07	0.06	0.01
Al_2O_3	0.70	0.98	0.65	0.66	0.67
Cr_2O_3	0.05	0.07	0.02	0.08	0.09
FeO*	9.85	10.80	10.03	10.32	10.22
MnO	0.12	0.09	0.09	0.10	0.13
MgO	32.53	31.64	32.40	32.05	32.41
CaO	0.39	0.29	0.29	0.31	0.28
Na_2O	0.00	0.01	0.00	0.02	0.01
Sum	99.84	99.60	99.78	99.32	99.67
cations per 6 oxygen atoms					
Si	1.971	1.966	1.974	1.971	1.968
Ti	0.002	0.002	0.002	0.001	0.000
Al	0.029	0.041	0.027	0.027	0.028
Cr	0.002	0.002	0.001	0.002	0.002
Fe	0.289	0.319	0.295	0.305	0.301
Mn	0.003	0.003	0.003	0.003	0.004
Mg	1.702	1.666	1.696	1.689	1.702
Ca	0.015	0.011	0.011	0.012	0.010
Na	0.000	0.001	0.000	0.001	0.000
Sum	4.012	4.010	4.009	4.013	4.017
% Ca	0.7	0.6	0.5	0.6	0.5
% Mg	84.9	83.5	84.7	84.2	84.5
% Fe	14.4	16.0	14.7	15.2	14.9
Mg#	85.5	83.9	85.2	84.7	85.0

* Total Fe as FeO

1.45 to 1.87 wt. %, and TiO_2 from 0.07 to 0.11 wt. %. Among the primary silicates in the Biskupice pyroxenite, clinopyroxene displays the highest values of, and smallest variation in, Mg#, which range from 87.0 to 88.4 (Figs 5 and 6). The Cr_2O_3 contents are low, ranging from 0.10 to 0.48 wt. %, with the highest values occurring in websterite H (Fig. 6; plotted in terms of Cr# and Mg#). However, like garnet, clinopyroxene in layer F contains almost no Cr (0.01 wt. % Cr_2O_3).

Amphibole is pargasite, with 0.15–1.93 wt. % TiO_2, 0.25–1.31 wt. % Cr_2O_3, and very little K_2O, < 0.2 wt. % (Tab. 5, Fig. 5). Values of Mg# vary slightly from 88.6 to 91.8.

5. Equilibration conditions

Temperatures in the Biskupice garnet pyroxenite were calculated by two Fe–Mg exchange geothermometers (garnet–orthopyroxene, Harley 1984; garnet–clinopyroxene, Powell 1985) and three two-pyroxene geothermometers (Bertrand and Mercier 1985; Brey and Köhler 1990; Taylor 1998); the pressures were estimated by two Al-in-orthopyroxene geobarometers (Brey and Köhler 1990; Nickel and Green 1985). Temperature and pressure estimates were obtained from the mean compositions of garnet, orthopyroxene, and clinopyroxene in layers B, D, and G, and three domains in layer H, because of its modal heterogeneity (Tab. 6). Layers B, D, and H were chosen because orthopyroxene, which is critical for estimating pressure, is a major phase in these layers, and layer G was included for comparison. All Fe was taken to be Fe^{2+}, due to the uncertainty in calculating Fe^{3+} from electron-microprobe (EMP) analyses and the relatively low concentrations of Fe in clinopyroxene, which is a procedure commonly followed in estimating temperatures and pressures for mantle peridotite and pyroxenite (Medaris 1999).

The two Fe–Mg exchange geothermometers give similar results for each layer, within 18 to 51 ºC of each other, and among the layers, with a mean of 881 ± 27(1σ) ºC at an assumed pressure of 35 kbar (Tab. 6). The three two-pyroxene geothermometers also yield comparable results within and among the layers, although the Bertrand and Mercier (1985) method consistently gives temperatures ~40–50 ºC below those of the other two methods. The mean temperature for all layers from the Brey and Köhler (1990) and the Taylor (1998) methods is 845 ± 22 ºC at 35 kbar, which is slightly below, but within error of, the mean estimate from Fe–Mg exchange geothermometry.

The two Al-in-orthopyroxene geobarometers also yield similar results for each layer, within 0.1 to 1.8 kbar of each other, and among the layers, with a mean of 38.3 ± 1.2 kbar at 900 ºC (Tab. 6).

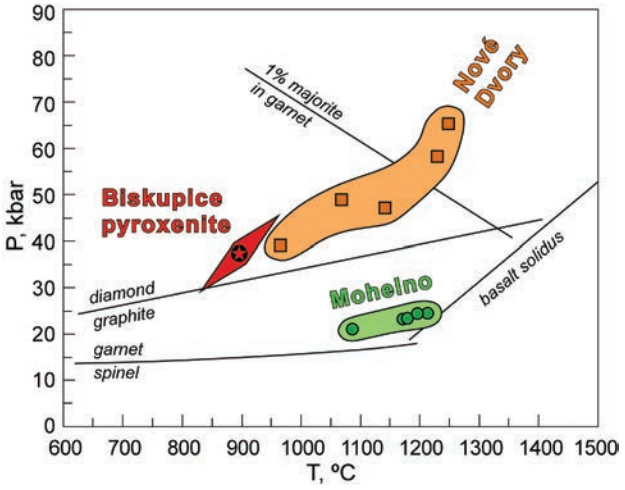

Fig. 7 Pressure–temperature estimate for the Biskupice garnet pyroxenite (star symbol and red polygon). Shown for comparison are field gradients for the Nové Dvory and Mohelno peridotites (Medaris et al. 2005). Garnet–spinel boundary in peridotite from O'Neill (1981), diamond–graphite boundary from Day (2012), majorite isopleth from Gasparik (2003), and anhydrous basalt solidus from Yasuda et al. (1994).

Tab. 4 Electron-microprobe analyses of clinopyroxene (means, grain cores)

Layer	A	B	C	D	E	F	G	H
wt. %								
SiO_2	53.64	54.12	54.02	54.08	54.12	54.08	53.97	53.88
TiO_2	0.11	0.09	0.09	0.11	0.08	0.11	0.10	0.07
Al_2O_3	1.72	1.50	1.45	1.76	1.77	1.87	1.71	1.69
Cr_2O_3	0.22	0.16	0.24	0.17	0.10	0.01	0.39	0.48
FeO*	3.94	3.91	3.86	3.99	4.27	4.29	4.24	3.97
MnO	0.06	0.03	0.07	0.06	0.07	0.03	0.05	0.07
MgO	16.28	16.69	16.54	16.39	16.09	16.28	16.10	16.13
CaO	22.38	22.06	21.94	21.96	21.64	21.79	21.71	21.85
Na_2O	0.82	1.03	1.07	1.06	1.26	1.13	1.27	1.29
Sum	99.17	99.58	99.27	99.58	99.40	99.60	99.54	99.44
cations per 6 oxygen atoms								
Si	1.973	1.980	1.982	1.978	1.985	1.979	1.979	1.977
Ti	0.003	0.002	0.002	0.003	0.002	0.003	0.003	0.002
Al	0.075	0.065	0.063	0.076	0.077	0.081	0.074	0.073
Cr	0.006	0.005	0.007	0.005	0.003	0.000	0.011	0.014
Fe	0.121	0.120	0.118	0.122	0.131	0.131	0.130	0.122
Mn	0.002	0.001	0.002	0.002	0.002	0.001	0.002	0.002
Mg	0.893	0.910	0.905	0.894	0.879	0.888	0.880	0.882
Ca	0.882	0.865	0.863	0.861	0.850	0.854	0.853	0.859
Na	0.058	0.073	0.076	0.075	0.090	0.080	0.090	0.092
Sum	4.013	4.020	4.018	4.016	4.018	4.018	4.021	4.024
% Ca	46.5	45.6	45.7	45.9	45.7	45.6	45.8	46.1
% Mg	47.1	48.0	48.0	47.6	47.3	47.4	47.2	47.4
% Fe	6.4	6.3	6.3	6.5	7.0	7.0	7.0	6.5
Mg#	88.0	88.4	88.4	88.0	87.0	87.1	87.1	87.9

* Total Fe as FeO

By combining the two Fe–Mg exchange geothermometers with the two Al-in-orthopyroxene geobarometers, one obtains a range of values among the layers from 873 ºC/34.9 kbar to 959 ºC/41.5 kbar, with a grand mean over all the layers of 894 ºC/37.4 kbar (Tab. 6). These results for the Biskupice garnet pyroxenite are consistent with the high P/T conditions for the Nové Dvory type of peridotite, plotting at the lower end of the P/T field gradient defined by the Nové Dvory peridotite itself (Fig. 7). Interestingly, the Nové Dvory field gradient and the Biskupice pyroxenite lie entirely within the diamond stability field, according to the revised diamond-graphite transition boundary (Day 2012).

6. Geochemistry

6.1. Major and minor elements in the layers

Major- and minor-element chemistries of the layers were calculated from modes of the layers and compositions of the constituent minerals (Tab. 1). Garnet, orthopyroxene, clinopyroxene, and amphibole were analyzed by EMP, and rutile and ilmenite were assumed to have end-member compositions.

Not surprisingly, the major-element compositions and Mg numbers of the Biskupice layers reflect the proportions of their three major constituent minerals, garnet, clinopyroxene, and orthopyroxene. The chemistries of clinopyroxenite layers A, C, E, F, and G plot between those of clinopyroxene and garnet, orthopyroxenite layers B and D between orthopyroxene and garnet, garnetite F between garnet and clinopyroxene, and websterite layer H within the clinopyroxene–orthopyroxene–garnet triangle (Fig. 8). In general, the layer compositions lie outside, or at the periphery, of the compositional field for pyroxenites in other Gföhl peridotites. Also shown for comparison in Fig. 8 are the compositions of pyroxenites from the Horní Bory locality (Ackerman et al. 2009). These pyroxenites belong to a strongly layered association of dunite, wehrlite, and pyroxenite, although the pyroxenites themselves are not internally layered.

Tab. 5 Electron-microprobe analyses of amphibole (means, grain cores)

Layer	A	C	E	G	H
wt. %					
SiO_2	43.78	43.99	42.15	46.05	43.61
TiO_2	1.93	0.48	0.15	0.44	0.59
Al_2O_3	12.99	13.51	16.47	11.81	13.65
Cr_2O_3	0.77	0.54	0.25	0.37	1.31
FeO*	5.72	5.40	6.21	5.81	5.06
MnO	0.06	0.08	0.08	0.06	0.05
MgO	16.54	17.01	16.47	17.49	16.65
CaO	11.36	11.28	10.98	11.13	11.26
Na_2O	2.72	2.67	3.14	2.80	2.79
K_2O	0.16	0.18	0.00	0.11	0.17
Sum	96.03	95.15	95.92	96.07	95.14
cation formula**					
Si	6.312	6.360	6.063	6.583	6.319
Al IV	1.688	1.640	1.937	1.417	1.681
sum T	8.0	8.0	8.0	8.0	8.0
Al VI	0.519	0.662	0.856	0.573	0.650
Ti	0.209	0.052	0.016	0.047	0.064
Fe^{3+}	0.232	0.324	0.378	0.319	0.281
Cr	0.088	0.062	0.029	0.042	0.150
Mg	3.554	3.667	3.533	3.727	3.597
Fe^{2+}	0.391	0.223	0.179	0.284	0.253
Mn	0.007	0.010	0.009	0.008	0.007
sum C	5.0	5.0	5.0	5.0	5.0
Mg	0.000	0.000	0.000	0.000	0.000
Fe^{2+}	0.066	0.105	0.190	0.091	0.080
Mn	0.000	0.000	0.000	0.000	0.000
Ca	1.755	1.748	1.692	1.705	1.749
Na	0.179	0.147	0.118	0.204	0.171
sum B	2.0	2.0	2.0	2.0	2.0
Na	0.580	0.602	0.759	0.572	0.612
K	0.030	0.034	0.001	0.020	0.032
sum A	0.610	0.635	0.759	0.592	0.643
Σ cations	15.610	15.635	15.759	15.592	15.643
Mg#	88.6	91.8	90.6	90.9	91.5

* total Fe as FeO
** calculated following the method of Schumacher (1997)

Most of the minor elements also reflect the layer modes. The highest contents of TiO_2 (0.60–0.73 wt. %) occur in layers with the most abundant rutile and ilmenite, Na_2O contents correlate with the amount of clinopyroxene, being highest in clinopyroxenite, and MnO is highest in garnetite (Tab. 1). In contrast with such behavior, Cr_2O_3 shows no correlation with modal composition. Layers A, C, G, and H contain 0.34–0.39 wt. % Cr_2O_3, layers B, D, and E contain 0.10–0.18 wt. %, but garnetite layer F is almost devoid of Cr_2O_3, having only 0.02 wt. % (Tab. 1).

6.2. Trace elements

6.2.1. Minerals

The cores and rims of garnet, clinopyroxene, and orthopyroxene in layers A, B, C, D, E, and F were analyzed for rare earth elements (REE), Y, and Cr (Tab. 7) using the laser-ablation ICP-MS technique. No systematic compositional differences were found between cores and rims of the three mineral species.

The REE concentrations in garnet are similar in all six layers, and the normalized patterns are characteristically enriched in the heavy REE (HREE) and depleted in the light REE (LREE) (Fig. 9). The HREE are ~10×PM (PM, Primitive Mantle; McDonough and Sun 1995), and the LREE decrease from ~5×PM in Sm to less than 0.1×PM in La.

The REE concentrations in clinopyroxene from the six layers are also mutually similar, with the normalized REE patterns being convex upward (Fig. 9), which is typical of clinopyroxene, with a maximum of ~10×PM at Nd and decreasing to ~1.5×PM at La and ~0.1×PM at Lu. Both clinopyroxene and garnet exhibit slight negative Eu anomalies; the mean value for Eu/Eu* is 0.86 ± 0.05 in clinopyroxene and 0.86 ± 0.02 in garnet.

The REE concentrations in orthopyroxene are near the detection limits of the analytical technique and are mostly lower than 0.1×PM, with the LREE being more depleted than the HREE (Fig. 9).

Electron-microprobe analyses demonstrated that Cr_2O_3 contents in garnet and clinopyroxene are very low in layer F compared to those in other layers, and this is confirmed by LA-ICP-MS analyses. Chromium contents in garnet F are 264 to 436 ppm, compared to a range of 1468 to 4390 ppm in the other layers, and Cr content in clinopyroxene F is 189 ppm, compared to 804 to 1220 ppm in the other layers (Tab. 7).

6.2.2. Layers

As is the case of the major elements, the trace-element compositions of the layers reflect their various modes. The REE patterns of the layers are controlled by the ratio of garnet to clinopyroxene, with REE-poor orthopyroxene acting simply as a dilutant. Consequently, the REE patterns for garnetite F and orthopyroxenites B and D are subparallel to that for garnet, whereas the pattern for clinopyroxenite G, which has the lowest garnet : clinopyroxene ratio among the layers, is subparallel to that for clinopyroxene (Fig. 10). Clinopyroxenites A, C, and E

Tab. 6 Temperature–pressure estimates for layers in the Biskupice garnet pyroxenite

Layer	B	D	G	H1	H2	H3
T ºC, Fe–Mg exchange geothermometers at 35 kbar						
Harley (1984)	938	902	851	850	856	881
Powell (1985)	915	873	902	882	871	863
					mean	881*(27)*
T ºC, two-pyroxene geothermometers at 35 kbar						
Bertrand and Mercier (1985)	805	806	814	793	784	788
Brey and Köhler (1990)	871	868	876	844	826	836
Taylor (1998)	858	861	849	825	813	816
					mean	845*(22)*
P kbar, Al-in-orthopyroxene geobarometers at 900 ºC						
Brey and Köhler (1990)	37.9	39.9	36.2	39.4	39.3	36.7
Nickel and Green (1985)	37.6	38.9	38.0	39.3	39.6	37.3
					mean	38.3*(1.2)*
*Iterative solution**						
T ºC	959*(33)*	915*(43)*	873*(44)*	876*(22)*	873*(10)*	874*(16)*
P kbar	41.5*(2.3)*	38.0*(1.6)*	34.9*(3.9)*	37.6*(1.7)*	37.4*(1.2)*	35.2*(1.3)*
					grand mean	894*(35)*
						37.4*(2.4)*

* grand mean values from combining the Harley and Powell geothermometers with the Brey and Köhler and Nickel and Green geobarometers; values for 1σ italicised in parentheses

and websterite H have intermediate patterns, displaying the convex upward shape of clinopyroxene, combined with higher levels of HREE. In contrast to garnet and clinopyroxene, the layers show no Eu anomaly, with a mean value for Eu/Eu* of 0.99 ± 0.03 over a range of 0.96 to 1.05.

In an extended multielement plot, all the layers exhibit anomalies in the high field strength elements (HFSE) and U (Fig. 11). The magnitudes of Nb, Ta, Zr, and Hf anomalies vary with the rock type, due to the distinct proportions of garnet and clinopyroxene in the layers and the different partition coefficients between garnet and clinopyroxene for the elements in question, sc. D_{Nb}(cpx/grt) > D_{Ta}(cpx/grt) and D_{Zr}(cpx/grt) < D_{Hf}(cpx/grt) (Green et al. 2000). For example, in layers with a high proportion of clinopyroxene relative to garnet (A, C, E, G, and H) the ratio of normalized Nb/Ta is ≥ 1, and the ratio of Zr/Hf is < 1, whereas in layers with a high proportion of garnet relative to clinopyroxene (F, B, and D) the ratio of Nb/Ta is < 1 and the ratio of Zr/Hf is ~ 1 (Fig. 11). In

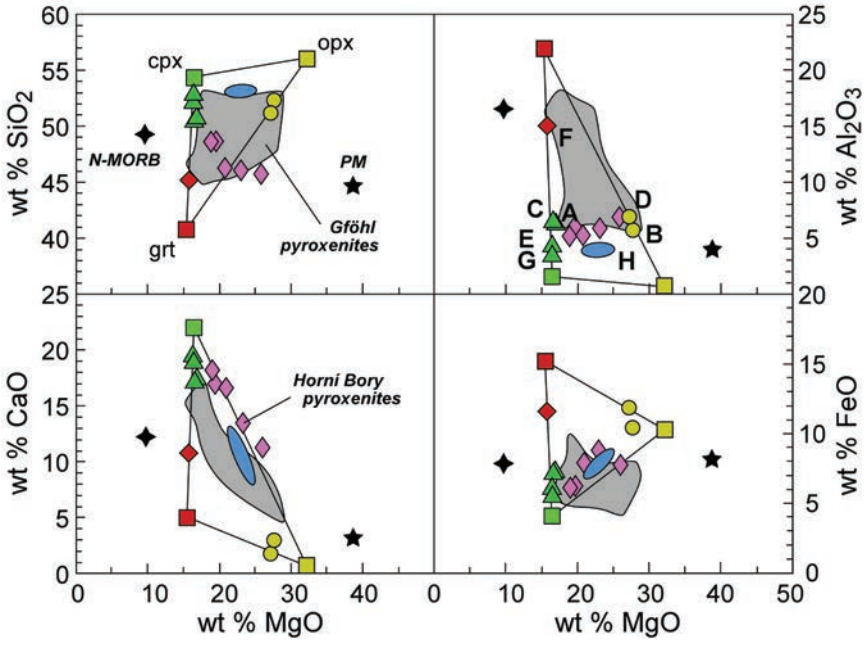

Fig. 8 Major oxide variation diagrams for Biskupice layers and minerals. Green triangles, clinopyroxenite layers A, C, E, G; yellow circles, orthopyroxenite layers B, D; red diamond, garnetite layer F; blue field, websterite layer H. Shown for comparison are the compositional fields for Gföhl pyroxenites (Medaris et al. 1995) and compositions of Horní Bory pyroxenites (Ackerman et al. 2009), as well as compositions of Primitive Mantle (PM) and N-MORB (McDonough and Sun 1995).

Tab. 7 Trace-element compositions of minerals (concentrations in ppm)

Layer	A				B				C			D			E		F		
Mineral	grt	grt	cpx	cpx	grt	grt	opx	opx	grt	grt	cpx	cpx	grt	grt	opx	opx	cpx	cpx	grt	grt	cpx
Location	core	rim	core	rim	core	rim	core	rim	core	rim	core	rim	core	rim	core	rim	core	rim	core	rim	core
Cr	4390	3660	1220	1180	1468	3151	299	327	3533	3386	1096	1108	2233	2093	321	202	981	804	436	264	189
Y	51.9	47.0	3.48	4.08	42.6	38.7	0.219	0.167	40.4	44.0	2.90	0.810	37.1	46.1	0.627	0.175	3.68	3.29	39.2	37.9	2.89
La	0.023	0.031	0.957	1.08	0.013	0.038	0.014	0.008	0.011	0.008	0.796	0.790	0.009	b.d.	0.009	0.024	1.15	1.08	0.024	0.043	0.889
Ce	0.113	0.263	5.13	5.76	0.064	0.191	0.019	0.022	0.050	0.063	4.17	4.24	0.054	0.200	0.017	0.052	6.25	5.63	0.144	0.124	5.05
Pr	0.072	0.073	1.46	1.68	0.057	0.100	0.004	0.006	0.043	0.056	1.17	1.28	0.048	0.122	0.004	0.005	1.81	1.60	0.064	0.052	1.48
Nd	1.29	1.13	11.1	11.7	1.07	1.34	0.028	0.027	0.897	0.919	9.17	9.20	0.981	2.25	0.011	0.034	13.30	11.96	1.13	0.800	10.51
Sm	1.79	1.59	3.15	3.57	1.54	1.64	0.023	0.007	1.34	1.39	2.57	2.68	1.54	2.62	0.023	0.024	3.88	3.51	1.72	1.41	3.00
Eu	0.868	0.782	0.829	0.835	0.754	0.820	0.005	0.007	0.669	0.687	0.625	0.680	0.764	1.11	0.011	0.006	0.990	0.950	0.810	0.790	0.889
Gd	4.94	4.26	2.55	2.53	4.21	4.32	0.022	0.015	3.73	3.64	2.09	2.18	4.156	5.98	0.060	0.035	2.93	2.82	4.32	4.27	2.56
Tb	1.10	0.97	0.269	0.290	0.931	0.924	0.007	0.004	0.814	0.887	0.216	0.250	0.921	1.22	0.013	0.007	0.318	0.291	0.965	1.00	0.275
Dy	8.75	7.92	1.14	1.17	7.42	6.81	0.038	0.032	6.79	7.27	1.02	0.980	6.95	8.45	0.116	0.039	1.28	1.20	7.33	7.39	1.13
Ho	1.92	1.76	0.140	0.150	1.62	1.46	0.007	0.008	1.55	1.73	0.123	0.130	1.52	1.70	0.023	0.009	0.160	0.140	1.58	1.63	0.141
Er	5.46	5.02	0.240	0.270	4.51	3.96	0.029	0.017	4.79	5.95	0.183	0.220	4.40	4.72	0.085	0.035	0.236	0.244	4.60	4.64	0.236
Tm	0.798	0.727	0.029	0.019	0.653	0.547	0.004	0.003	0.727	0.964	0.022	0.021	0.637	0.650	0.010	0.002	0.019	0.021	0.692	0.730	0.032
Yb	5.16	4.61	0.100	0.100	4.22	3.40	0.022	0.017	5.07	7.24	0.056	0.090	4.31	4.18	0.108	0.033	0.096	0.090	4.57	4.38	0.089
Lu	0.738	0.659	0.006	0.014	0.596	0.493	0.002	0.004	0.866	1.22	0.013	0.011	0.656	0.610	0.015	0.005	0.010	0.011	0.754	0.696	0.014

b.d., below detection

contrast, all the layers except orthopyroxenite exhibit a negative Ti anomaly, and all show a pronounced positive U anomaly.

6.3. Isotopes

6.3.1. Oxygen isotopes

Ratios for $^{18}O/^{16}O$ were determined by laser fluorination for garnet separates from all the layers, including two domains in layer H (analytical details are given in the Appendix). Two measurements of garnet were made for each layer and domain; the average values of $\delta^{18}O_{VSMOW}$ range from 5.44 ‰ to 5.65 ‰, with a mean for all the samples of 5.49 ± 0.13 ‰ (2 SD; Tab. 9). Although the $\delta^{18}O$ values for garnet in orthopyroxenites B and D are slightly higher than those in other layers, 5.55 ‰ and 5.65 ‰ *vs.* ≤ 5.49 ‰, all the results are almost within error of each other. The mean $\delta^{18}O$ value for garnet in the Biskupice pyroxenite, 5.49 ± 0.13 ‰, is the same within error as that for garnet in peridotite xenoliths, 5.42 ± 0.5 ‰ (Wang et al., 2011). Values of $\delta^{18}O$ for garnet in pyroxenite from three peridotite bodies elsewhere in the Gföhl Assemblage (Nihov, Nové Dvory, and Bečváry) are slightly isotopically lighter than those from Biskupice, at 4.87, 4.91, and 5.15 ‰ (Medaris et al. 1995).

6.3.2. Neodymium and strontium isotopes

Neodymium isotopes were measured for garnet and clinopyroxene from clinopyroxenite layers A and E, garnetite F, and websterite H, and Sr isotopes were determined for clinopyroxene from layers E, F, and H (Tab. 10). Rubidium concentrations were not determined in clinopyroxene, because they are commonly very low (< 1 ppm) in pyroxenitic clinopyroxene, and such low levels would not affect $^{87}Sr/^{86}Sr$ ratios significantly.

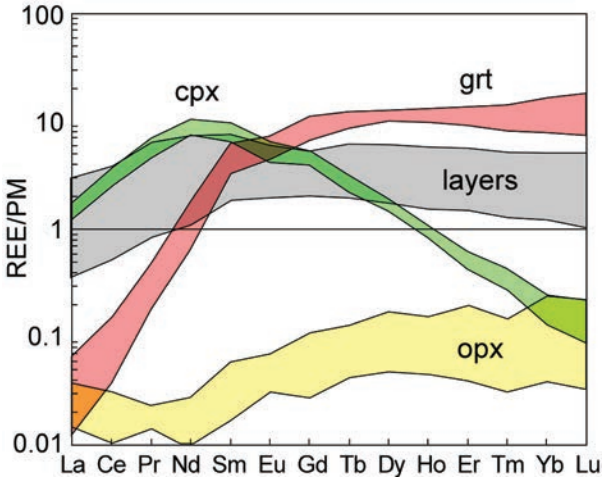

Fig. 9 Rare earth element compositions of garnet, clinopyroxene, and orthopyroxene, normalized to Primitive Mantle, PM (McDonough and Sun 1995).

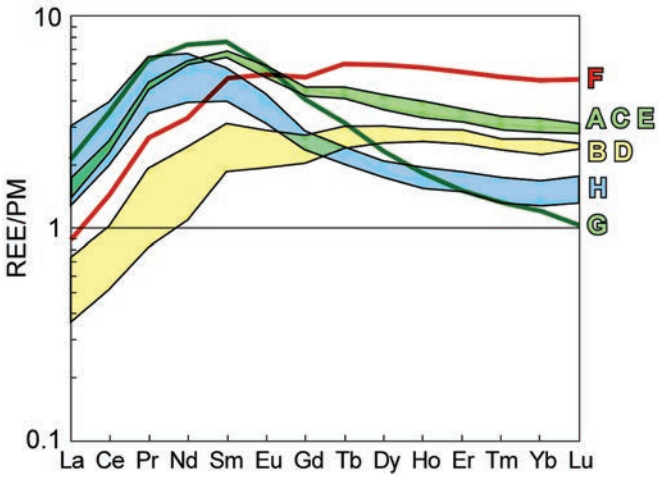

Fig. 10 Rare earth element compositions of layers in the Biskupice pyroxenite, normalized to Primitive Mantle, PM (McDonough and Sun 1995). Yellow, orthopyroxenite; green, clinopyroxenite; blue, websterite; red, garnetite.

Tab. 8 Trace-element compositions of layers (concentrations in ppm)

Layer	A	B	C	D	E	F	G	H1	H2	H3
Sc	59	48	60	32	48	47	42	47	59	53
Ti	3350	3688	3136	3578	3120	4015	1570	1785	1461	1392
V	231	158	252	140	257	245	246	159	195	197
Cr	1936	1445	1852	1091	1229	77	2177	2576	244	2108
Co	54	87	60	97	62	68	49	75	55	50
Ni	329	525	423	652	356	167	374	523	382	451
Zn	101	221	141	168	148	83	77	115	101	89
Rb	0.92	1.04	0.83	0.97	0.94	0.86	0.62	1.59	1.13	1.56
Sr	132	48	111	18	110	57	145	96	158	237
Y	13.3	11.7	15.2	10.1	13.3	22.2	6.9	6.3	7.7	6.9
Zr	37	38	32	28	37	55	30	20	20	18
Nb	0.61	0.51	1.12	0.58	0.29	0.95	0.55	0.69	0.42	0.39
La	1.11	0.48	0.91	0.24	0.96	0.57	1.36	0.85	1.39	1.97
Ce	4.37	1.73	3.82	0.87	4.24	2.43	5.84	3.39	5.27	6.66
Pr	1.26	0.49	1.15	0.21	1.25	0.68	1.59	0.90	1.34	1.66
Nd	7.69	3.02	7.08	1.37	7.60	4.16	9.20	4.99	7.14	8.44
Sm	2.63	1.27	2.62	0.76	2.79	2.08	3.08	1.64	2.15	2.32
Eu	0.79	0.45	0.83	0.30	0.89	0.83	0.90	0.48	0.62	0.66
Gd	2.30	1.50	2.56	1.10	2.49	2.80	2.20	1.29	1.55	1.56
Tb	0.41	0.30	0.46	0.24	0.42	0.59	0.31	0.20	0.24	0.23
Dy	2.51	2.04	2.87	1.71	2.47	4.01	1.54	1.18	1.42	1.25
Ho	0.52	0.44	0.59	0.38	0.50	0.86	0.27	0.23	0.29	0.25
Er	1.44	1.27	1.60	1.09	1.39	2.40	0.66	0.65	0.82	0.67
Tm	0.20	0.18	0.23	0.16	0.21	0.35	0.09	0.09	0.12	0.09
Yb	1.25	1.16	1.45	0.98	1.33	2.20	0.53	0.59	0.75	0.57
Lu	0.19	0.17	0.21	0.16	0.20	0.34	0.07	0.09	0.12	0.09
Hf	1.27	1.42	1.09	0.77	1.44	1.45	1.21	0.73	0.64	0.58
Ta	0.041	0.064	0.045	0.072	0.048	0.095	0.035	0.019	0.015	0.011
Pb	50	53	49	22	21	23	14	11	9	12
Th	0.19	0.21	0.29	0.20	0.18	0.24	0.17	0.13	0.14	0.21
U	1.29	1.93	4.34	1.87	1.86	1.58	2.04	2.09	0.91	0.88

Tab. 9 Oxygen isotope ratios for garnet

Layer	$\delta^{18}O^{*}$ ‰ VSMOW	Duplicate Analyses
A	5.47	5.43; 5.50
B	5.55	5.56; 5.53
C	5.47	5.37; 5.56
D	5.65	5.76; 5.53
E	5.49	5.55; 5.53
F	5.47	5.49; 5.45
G	5.49	5.51; 5.46
H1	5.44	5.48; 5.39
H2	5.45	5.43; 5.41
all**	5.49 ± 0.13	

* values are averages of two measurements in each layer
** mean value and 2σ for all layers
UWG-2 garnet standard analyses
Raw Average = 5.74 ± 0.10 ‰ (2σ, N = 6)

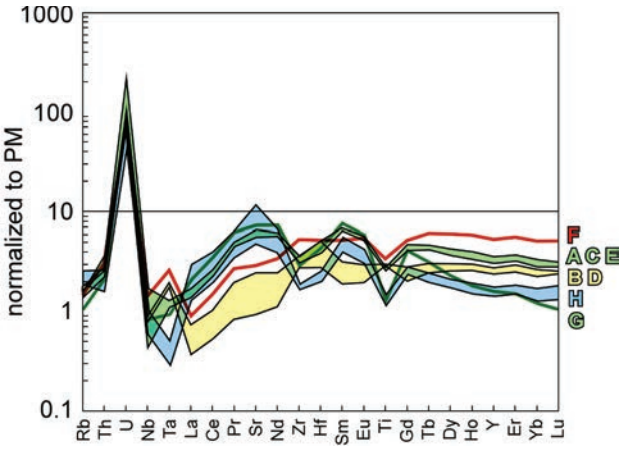

Fig. 11 Extended plot of trace-element compositions of layers in the Biskupice pyroxenite, normalized to Primitive Mantle, PM (McDonough and Sun 1995). Layers are color coded as in Fig. 10.

Isotopic ratios among the layers are closely similar; values for $^{87}Sr/^{86}Sr$ range from 0.70496 to 0.70501, and initial ε_{Nd} values for the different layers are analytically indistinguishable and range from +1.8 to +2.2 (Tabs 10–11). In a plot of ε_{Nd}^{335} vs. $(^{87}Sr/^{86}Sr)_{335}$, such values fall within the oceanic mantle array and at an intermediate position along the trend defined by pyroxenites and eclogites in other Gföhl peridotite bodies (Fig. 12).

7. Sm–Nd geochronology

The Sm–Nd isotope analyses of garnet–clinopyroxene pairs in layers A, E, F, and H yield the same age within error, ranging from 329 ± 5 to 334 ± 3 Ma (Tab. 11; Fig. 13). An isochron fit for all the garnet and pyroxene pairs yields an age of 332.1 ± 1.6 Ma with a MSWD of 1.7. This age is the same within error as the mean age for nine pyroxenites and eclogites in other Gföhl peridotite

Tab. 10 Nd and Sm concentrations and present-day Nd and Sr isotopic ratios for garnet and clinopyroxene

Layer	Mineral	Nd, ppm	Sm, ppm	Sm/Nd	$^{147}Sm/^{144}Nd$	2σ	$^{143}Nd/^{144}Nd$	2σ	$^{87}Sr/^{86}Sr$	2σ
A	grt	0.9806	1.4509	1.479604	0.89488	0.00179	0.514250	0.000018		
A	cpx	9.8540	2.9247	0.296803	0.17944	0.00036	0.512708	0.000011	n.d.	
E	grt	1.0145	1.5400	1.517989	0.91810	0.00184	0.514305	0.000006		
E	cpx	11.1634	3.4944	0.313023	0.18925	0.00038	0.512717	0.000011	0.704964	0.000007
F	grt	0.7154	1.1319	1.582192	0.95695	0.00191	0.514387	0.000009		
F	cpx	10.2216	3.2300	0.315997	0.19105	0.00038	0.512714	0.000012	0.704975	0.000001
H	grt	0.9621	1.2576	1.307141	0.79052	0.00158	0.514012	0.000015		
H	cpx	9.2731	2.6303	0.283648	0.17149	0.00034	0.512674	0.000012	0.705007	0.000013

n.d., not determined

Tab. 11 Ages, initial $^{143}Nd/^{143}Nd$ ratios, and values of ε_{Nd}^{335} for selected layers in the Biskupice garnet pyroxenite

Layer	Age, Ma	$^{143}Nd/^{144}Nd_{335}$	2σ	ε_{Nd}
A	329.2 ± 4.5	0.512321	0.000014	2.15
E	332.8 ± 2.7	0.512305	0.000014	1.93
F	333.6 ± 3.0	0.512297	0.000015	1.80
H	330.1 ± 4.7	0.512303	0.000016	1.82
all (MSWD = 1.7)	332.1 ± 1.6	0.512306	0.000007	*1.93*

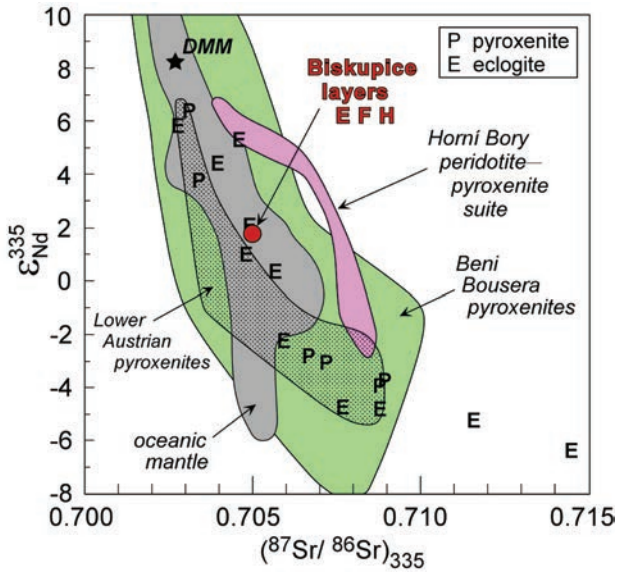

Fig. 12 ε_{Nd}^{335} *vs.* $(^{87}Sr/^{86}Sr)_{335}$ for clinopyroxene in Biskupice layers E, F, and H (red circle). Shown for comparison are values for clinopyroxene in pyroxenite (P) and eclogite (E) in other Gföhl garnet peridotites (Medaris et al. 2006). Also plotted are the compositions of depleted MORB mantle (DMM; Hart 1988), and compositional fields for oceanic mantle (Hart 1988), Gföhl pyroxenites in Lower Austria (Becker 1996), the Horní Bory peridotite–pyroxenite suite (Ackerman et al. 2009), and Beni Bousera pyroxenites (Pearson et al. 1993).

bodies (336 ± 7 Ma), although older Sm–Nd ages of 370 ± 15, 373 ± 7, and 377 ± 20 Ma have been obtained from garnet pyroxenites at Mitterbachgraben, Níhov, and Bečváry, respectively (Carswell and Jamtveit 1990; Brueckner et al. 1991; Beard et al. 1992; Becker 1997; Medaris et al. 1995).

8. Discussion

The pronounced mineralogical layering (Fig. 2) and major- and trace-element compositions (Figs 8, 10–11) in the Biskupice pyroxenite are consistent with the layers having originated as high-pressure crystal cumulates. A similar origin has been demonstrated for other peridotite-hosted garnet pyroxenites in the Bohemian Massif (Medaris et al. 1995) and for garnet pyroxenite xenoliths, based on oxygen isotope and trace-element constraints (Gonzaga et al. 2010; Ackerman et al. 2012). The layers could not have formed by recrystallization of low-pressure assemblages of olivine, clinopyroxene, and plagioclase, because the major-element compositions of some layers lie outside the compositional fields defined by these three phases. Also, the layers could not have formed by metamorphic differentiation of an initially chemically homogeneous material, because the Cr contents of garnet and clinopyroxene in layer F are vastly different from those in the other layers.

Although the compositions of melts from which the cumulates crystallized could be calculated from the cumulate mineral compositions, such a procedure is only valid if the cumulate phases have preserved their original, high-temperature compositions. However, this is not the case for minerals in the Biskupice pyroxenite, which have re-equilibrated at P–T conditions well below those of the basalt solidus (Fig. 7). Also, the ratios of D_{cpx}/D_{grt} for REE in layers A, C, and F have a steeper slope than those determined in high-temperature experiments (Fig. 14), indicating that minerals in the Biskupice pyroxenite have experienced re-equilibration of trace elements in addition

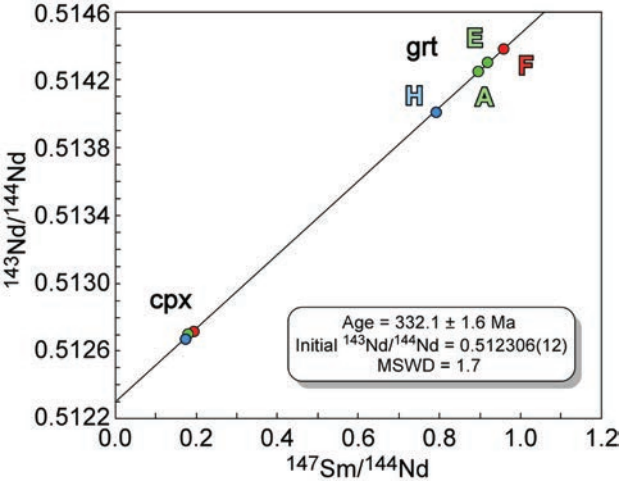

Fig. 13 Sm–Nd isochron for the Biskupice pyroxenite. Garnet and clinopyroxene pairs from layers A, E, F, and H. For illustrative purposes, the data symbols are shown larger than the actual errors. The 2σ error for the initial $^{143}Nd/^{144}Nd$ ratio is shown in brackets.

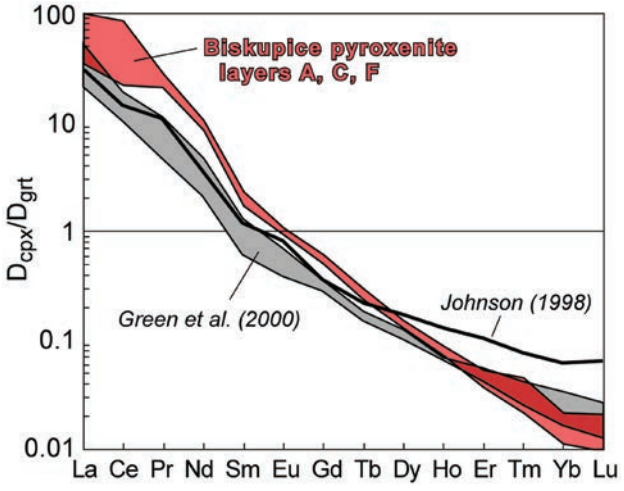

Fig. 14 Values of D_{cpx}/D_{grt} for the REE in Biskupice layers A, C, and F. Shown for comparison are experimentally determined values of D_{cpx}/D_{grt} at high temperatures (Johnson 1998; Green et al. 2000).

to major elements, which prohibits accurate determination of melt compositions from the present mineral chemistries.

In addition to compositional re-equilibration, the Biskupice pyroxenite has been thoroughly recrystallized, and any pre-existing igneous textures have been replaced by a subsolidus, granoblastic texture, although the original layering of the sample has been preserved. It is likely that the garnet clinopyroxenite and garnet orthopyroxenite layers were originally bimineralic accumulations of garnet and pyroxene (ignoring the accessory phases, rutile and ilmenite). The small amounts of orthopyroxene in clinopyroxenite probably originated through exsolution and segregation from a high-temperature, low-Ca clinopyroxene. Similarly, clinopyroxene in orthopyroxenite probably formed by exsolution and segregation from a high-temperature, high-Ca orthopyroxene. Reconstructed pyroxene compositions for a given layer were obtained by calculating a single pyroxene composition from the present compositions and modes of the two pyroxenes in that layer. For example, the reconstructed composition of clinopyroxene in clinopyroxenite contains ~21.2 wt. % CaO, compared to its present content of ~21.9 wt. % CaO, and that for reconstructed orthopyroxene in orthopyroxenite is ~1.5 wt. % CaO vs. ~0.3 wt. %.

Despite extensive re-equilibration and recrystallization, some qualitative conclusions regarding melt compositions may be drawn from the characteristics of the pyroxenite layers, experimental results on basalt crystallization, and comparison to pyroxenite occurrences elsewhere. Orthopyroxene is not a liquidus phase in basaltic melts at high pressure (Takahashi et al. 1998; Yasuda et al. 1994), which precludes crystallization of the Biskupice pyroxenite from a melt of basaltic composition. Reaction between basaltic melts and mantle peridotite has been demonstrated by Ackerman et al. (2009), and such resultant melts would have intermediate compositions capable of crystallizing orthopyroxene, garnet, and clinopyroxene at high pressure.

In many other Gföhl pyroxenites, the presence of Eu anomalies and $\delta^{18}O$ values greater, or less, than that in the mantle provide evidence for a crustal component in the melts from which the pyroxenites crystallized (Pearson et al. 1991, 1993; Medaris et al. 1995; Becker 1996; Gysi et al. 2011). On the basis of these parameters, however, no crustal component is required for the Biskupice pyroxenite, because $\delta^{18}O$ in Biskupice garnet is similar to that in the mantle (Tab. 9) and garnet and clinopyroxene only have slight negative Eu anomalies (Fig. 9). On the other hand, Nd and Sr isotopes indicate a crustal component in the Biskupice pyroxenite, whose ε_{Nd}^{335} and $(^{87}Sr/^{86}Sr)_{335}$ values are significantly displaced from that of depleted MORB mantle and plot at an intermediate position along the Nd and Sr isotopic trend for Gföhl pyroxenites and eclogites in the Czech Republic (Fig. 12). The Czech Gföhl pyroxenite and eclogite trend extends well beyond the mantle array and has been modeled by a mixture of mantle material with subducted oceanic crust, including oceanic clay (Medaris et al. 1995). A similar isotopic trend for Gföhl pyroxenites in Lower Austria (Fig. 12) has also been explained by a mixture of mantle and crust, but in this case, by continental crust (Becker 1996). The isotopic trend for the Gföhl pyroxenite–peridotite suite at the Horní Bory locality differs from those in the other Gföhl localities by having a convex upward configuration, which has been modeled by mixing between depleted mantle and Sr-rich melt from subducted oceanic crust (Ackerman et al. 2009).

The HFSE show negative anomalies in extended trace-element plots for some Gföhl pyroxenites (Becker 1996) as well as for the Horní Bory peridotite–pyroxenite suite (Ackerman et al. 2009), and such negative anomalies have been ascribed to an arc component in the melts from which the pyroxenites crystallized. The HFSE also tend to display negative anomalies in the Biskupice pyroxenite (Fig. 11), although the pattern is modified to some extent by the accumulation of different proportions of garnet and clinopyroxene in the different layers, suggesting the possibility of an arc component in this pyroxenite occurrence, as well.

The most prominent anomaly among trace elements in the Biskupice pyroxenite is displayed by U (Fig. 11). This large positive anomaly is not supported by the U contents of the primary silicate minerals, and most likely arises from the presence of U along grain boundaries. A similar strong positive U anomaly is displayed by Horní Bory pyroxenite (Ackerman et al. 2009). Such strong positive U anomalies (and low Th/U ratios) may have originated through the activity of late Variscan (270–290 Ma) hydrothermal fluids associated with the nearby Třebíč durbachite pluton (Kříbek et al. 2009).

9. Conclusions

Despite mm-scale recrystallization and re-equilibration at ~900 ºC and ~37 kbar, cm-scale layering has been preserved in the Biskupice garnet pyroxenite. The major- and trace-element compositions of the layers and their REE patterns are consistent with an origin of the layers by HT–HP crystallization and accumulation of different proportions of garnet, clinopyroxene, and orthopyroxene. The melt from which the phases crystallized is inferred to have resulted from reaction between basaltic magma and mantle peridotite and was probably intermediate in composition, allowing for crystallization of orthopyroxene and garnet at high pressure. The Nd and Sr isotopic compositions of the layers and the presence of negative anomalies for the HFSE indicate a crustal component

in the melt, perhaps derived from subducted crust. This exceptional layered pyroxenite thus encapsulates many of the petrogenetic features invoked for the origin of garnet pyroxenites elsewhere in the Gföhl Assemblage of the Moldanubian Zone in the Bohemian Massif.

Acknowledgements. We are indebted to John Fournelle for his expert advice and direction in electron probe microanalysis, and to Brian Hess for providing high-quality polished thin sections. This research was supported by Charles University Research Program MSM 0021620855 to Jelínek and National Science Foundation Grant EAR0838058 to Valley. We thank Ruth Gonzaga and Martin Racek for constructive reviews of the manuscript and Stanislav Vrána for editorial handling.

References

Ackerman L, Jelínek E, Medaris G Jr, Ježek J, Siebel W, Strnad L (2009) Geochemistry of Fe-rich peridotites and associated pyroxenites from Horní Bory, Bohemian Massif: insights into subduction-related melt–rock reactions. Chem Geol 259: 152–167

Ackerman L, Špaček P, Medaris G Jr, Hegner E, Svojtka M, Ulrych J (2012) Geochemistry and petrology of pyroxenite xenoliths from Cenozoic alkaline basalts, Bohemian Massif. J Geosci 58: 199–219

Armstrong JT (1988) Quantitative analysis of silicate and oxide materials: comparison of Monte Carlo, ZAF, and φ(ρz) procedures. In: Newbury DE (ed) Microbeam Analyses. Proceedings of the 23rd Annual Conference of the Microbeam Analysis Society, San Francisco Press, San Francisco, pp 239–246

Beard BL, Medaris LG Jr, Johnson CM, Brueckner HK, Mísař Z (1992) Petrogenesis of Variscan high-temperature Group A eclogites from the Moldanubian Zone of the Bohemian Massif, Czechoslovakia. Contrib Mineral Petrol 111: 468–183

Becker H (1996) Crustal trace element and isotopic signatures in garnet pyroxenites from garnet peridotite massifs from Lower Austria. J Petrol 37: 785–810

Becker H (1997) Sm–Nd garnet ages and cooling history of high-temperature garnet peridotite massifs and high-pressure granulites from lower Austria. Contrib Mineral Petrol 127: 224–236

Bertrand P, Mercier J–CC (1985) The mutual solubility of coexisting ortho- and clinopyroxene: toward an absolute geothermometer for the natural system? Earth Planet Sci Lett 76: 109–122

Brey GP, Köhler T (1990) Geothermobarometry in four-phase lherzolites II. New thermobarometers, and practical assessment of existing thermobarometers. J Petrol 31: 1352–1378

Brueckner HK, Medaris LG Jr, Bakun-Czubarow N (1991) Nd and Sr age and isotope patterns from Variscan eclogites of the eastern Bohemian Massif. Neu Jb Mineral, Abh 163: 169–196

Carswell DA, Jamtveit B (1990) Variscan Sm–Nd ages for the high-pressure metamorphism in the Moldanubian Zone of the Bohemian Massif, Lower Austria. Neu Jb Mineral, Abh 162: 69–78

Cháb J, Stráník Z, Eliáš M (2007) Geological map of the Czech Republic 1:500 000. Czech Geological Survey, Prague

Day HW (2012) A revised diamond–graphite transition curve. Amer Miner 97: 52–62

Gasparik T (2003) Phase Diagrams for Geoscientists – An Atlas of The Earth's Interior. Springer, Berlin, pp 1–350 pp

Gonzaga RG, Lowry D, Jacob DE, LeRoex A, Schulze D, Menzies MA (2010) Eclogites and garnet pyroxenites: similarities and differences. J Volcanol Geotherm Res 190: 235–247

Green TH, Blundy JD, Adam J, Yaxley GM (2000) SIMS determination of trace element partition coefficients between garnet, clinopyroxene and hydrous basaltic liquids at 2–7.5 GPa and 1080–1200 ºC. Lithos 53: 165–187

Griffin WL, O'Reilly SY (2007) Cratonic lithospheric mantle: is anything subducted? Episodes 30: 43–53

Gysi AP, Jagoutz O, Schmidt MW, Targuisti K (2011) Petrogenesis of pyroxenites and melt infiltrations in the ultramafic complex of Beni Bousera, northern Morocco. J Petrol 52: 1629–1735

Harley SL (1984) An experimental study of the partitioning of Fe and Mg between garnet and orthopyroxene. Contrib Mineral Petrol 86: 359–373

Harte SR (1988) Heterogeneous mantle domains: signatures, genesis and mixing chronologies. Earth Planet Sci Lett 90: 273–296

Hasalová P, Janoušek V, Schulmann K, Štípská P, Erban V (2008) From orthogneiss to migmatite: geochemical assessment of the melt infiltration model in the Gföhl Unit (Moldanubian Zone, Bohemian Massif). Lithos 102: 508–537

Holub FV, Machart J, Manová M (1997) The Central Bohemian Plutonic Complex: geology, chemical composition and genetic interpretation. Sbor geol Věd, ložisk Geol Mineral 31: 27–50

Jacob DE (2004) Nature and origin of eclogite xenoliths from kimberlites. Lithos 77: 295–316

Jacobsen SB, Wasserburg GJ (1980) Sm–Nd isotopic evolution of chondrites. Earth Planet Sci Lett 50: 139–155

Johan Z, Strnad L, Johan V (2012) Evolution of the Cínovec (Zinnwald) Granite Cupola, Czech Republic: composition of feldspars and micas, a clue to the origin of W, Sn mineralization. Canad Mineral 50: 1131–1148

Johnson KTM (1998) Experimental determination of partition coefficients for rare earth and high-field-strength

elements between clinopyroxene, garnet, and basaltic melt at high pressures. Contrib Mineral Petrol 133: 60–68

Kotková J, Schaltegger U, Leichmann J (2010) Two types of ultrapotassic plutonic rocks in the Bohemian Massif – coeval intrusions at different crustal levels. Lithos 115: 163–176

Kříbek B, Žák K, Dobeš P, Leichmann J, Pudilová M, René M, Scharm B, Scharmová M, Hájek A, Holeczy D, Hein UF, Lehmann B (2009) The Rožná uranium deposit (Bohemian Massif, Czech Republic): shear zone-hosted, late Variscan and post-Variscan hydrothermal mineralization. Miner Depos 44: 99–128

Kusbach V, Ulrich S, Schulmann K (2012) Ductile deformation and rheology of sub-continental mantle in a hot collisional orogeny: example from the Bohemian Massif. J Geodyn 56–57: 108–123

Kusiak MA, Dunkley DJ, Suzuki K, Kachlík V, Kedzior A, Lekki J, Opluštil S (2010) Chemical (non-isotopic) and isotopic dating of Phanerozoic zircon – a case study of durbachite from the Třebíč Pluton, Bohemian Massif. Gondwana Res 17: 153–161

Lapen TJ, Medaris LG Jr, Johnson CM, Beard BL (2005) Archean to Middle Proterozoic evolution of Baltica subcontinental lithosphere: evidence from combined Sm–Nd and Lu–Hf isotope analyses of the Sandvik ultramafic body, Norway. Contrib Mineral Petrol 150: 131–145

Lapen TJ, Medaris LG Jr, Beard BL, Johnson CM (2009) The Sandvik peridotite, Gurskøy, Norway: three billion years of mantle evolution in the Baltica lithosphere. Lithos 109: 145–154

Ludwig KR (2003) Isoplot/Ex version 3.41. A geochronological toolkit for Microsoft Excel, User's Manual. Berkeley Geochronology Center Special Publications 4

Lugmair G W, Marti K (1978) Lunar initial $^{143}Nd/^{144}Nd$: differential evolution line of the lunar crust and mantle. Earth Planet Sci Lett 39: 349–357

McDonough WF, Sun S (1995) The composition of the Earth. Chem Geol 120: 223–253

Medaris LG Jr (1999) Garnet peridotites in Eurasian high-pressure and ultrahigh-pressure terranes: a diversity of origins and thermal histories. Int Geol Rev 41: 799–815

Medaris LG Jr, Carswell DA (1990) The petrogenesis of Mg–Cr garnet peridotites in European metamorphic belts. In: Carswell DA (ed) Eclogite Facies Rocks. Blackie, Glasgow, pp 260–290

Medaris LG Jr, Wang HF, Mísař Z, Jelínek E (1990) Thermobarometry, diffusion modelling and cooling rates of crustal garnet peridotites: two examples from the Moldanubian Zone of the Bohemian Massif. Lithos 25: 189–202

Medaris LG Jr, Beard BL, Johnson CM, Valley JW, Spicuzza MJ, Jelínek E, Mísař Z (1995) Garnet pyroxenite and eclogite in the Bohemian Massif: geochemical evidence for Variscan recycling of subducted lithosphere. Geol Rundsch 84:489–505

Medaris G Jr, Wang H, Jelínek E, Mihaljevič M, Jakeš P (2005) Characteristics and origins of diverse Variscan peridotites in the Gföhl Nappe, Bohemian Massif, Czech Republic. Lithos 82: 1–23

Medaris LG Jr, Beard BL, Jelínek E (2006) Mantle–derived, UHP garnet pyroxenite and eclogite in the Moldanubian Gföhl Nappe, Bohemian Massif: a geochemical review, new P–T determinations and tectonic interpretation. Int Geol Rev 48: 765–777

Nakamura D, Svojtka M, Naemura K, Hirajima T (2004) Very high-pressure (>4 GPa) eclogite associated with the Moldanubian Zone garnet peridotite (Nové Dvory, Czech Republic). J Metamorph Geol 22: 593–603

Nickel KG, Green DH (1985) Empirical geothermobarometry for garnet peridotites and implications for the nature of the lithosphere, kimberlites and diamonds. Earth Planet Sci Lett 73: 158–170

Obata M, Hirajima T, Svojtka M (2006) Origin of eclogite and garnet pyroxenite from the Moldanubian Zone of the Bohemian Massif, Czech Republic and its implication to other mafic layers embedded in orogenic peridotites. Mineral Petrol 88: 321–340

O'Neill HStC (1981) The transition between spinel lherzolite and garnet lherzolite, and its use as a geobarometer. Contrib Mineral Petrol 77: 185–194

Pearson DG, Davies GR, Nixon PH, Greenwood PB, Mattey DP (1991) Oxygen isotope evidence for the origin of pyroxenites in the Beni Bousera peridotite massif, N. Morocco: derivation from subducted oceanic lithosphere. Earth Planet Sci Lett 102: 289–301

Pearson DG, Davies GR, Nixon PH (1993) Geochemical constraints on the petrogenesis of diamond facies pyroxenites from the Beni Bousera peridotite massif, North Morocco. J Petrol 34: 125–172

Powell R (1985) Regression diagnostics and robust regression in geothermometer/geobarometer calibration: the garnet–clinopyroxene geothermometer revisited. J Metamorph Geol 2: 33–42

Schumacher JC (1997) Appendix 2. The estimation of the proportion of ferric iron in the electron-microprobe analysis of amphiboles. Can Mineral 35: 238–246

Strnad L, Mihaljevič M, Šebek O (2005) Laser ablation and solution ICP–MS determination of rare earth elements in USGS BIR-1G, BHVO-2G and BCR-2G glass reference material. Geost Geoanal Res 29: 303–314

Takahashi E, Nakajima K, Wright TL (1998) Origin of the Columbia River basalts: melting model of a heterogeneous plume head. Earth Planet Sci Lett 162: 63–80

Taylor WR (1998) An experimental test of some geothermometer and geobarometer formulations for upper mantle peridotites with application to the thermobarom-

etry of fertile lherzolite and garnet websterite. Neu Jb Mineral, Abh 172: 381–408

Valley JW, Kitchen NE, Kohn MJ, Niendorf CR, Spicuzza MJ (1995) UWG-2, a garnet standard for oxygen isotope ratio: strategies for high precision and accuracy with laser heating. Geochim Cosmochim Acta 59: 5223–5231

Wang Z, Bucholz C, Skinner B, Shimizu N, Eiler J (2011) Oxygen isotope constraints on the origin of high-Cr garnets from kimberlites. Earth Planet Sci Lett 312: 337–347

Yasuda A, Fujii T, Kurita K (1994) Melting phase relations of an anhydrous mid-ocean ridge basalt from 3 to 20 GPa: implications for the behavior of subducted oceanic crust in the mantle. J Geophys Res 99 B5: 9401–9414